5. Structure of Rapamycin: An NMR and Molecular-Dynamics Investigation

by **Horst Kessler***, **Rainer Haessner**, and **Wolfgang Schüler**

Organisch-chemisches Institut, Technische Universität München, Lichtenbergstrasse 4, D–8046 Garching

(19.X.92)

The highly active immunosuppressive antibiotic rapamycin is a specific inhibitor of a signal transduction pathway that results in exocytosis and transcription. We report the results of the homo- and heteronuclear NMR experiments of rapamycin in DMSO leading to a complete assignment of the ^{1}H- and ^{13}C-NMR signals. With exception of one CH_2 group, all diastereotopic assignments could be achieved using heteronuclear long-range coupling constants. Restrained molecular-dynamics simulation in the same solvent as the NMR experiments led to a well defined conformation of the rapamycin molecule in solution. Differences between the solution and crystal structures are discussed.

Introduction. – The 21-membered macrocyclic lactone rapamycin [1] is a highly active inhibitor of specific signal-transduction pathways that lead to T-lymphocyte activation [2]. Whereas two further immunosuppressants (cyclosporin A [3] and FK506 [4]) are structurally well characterized, no structural analysis of the rapamycin molecule in solution was published.

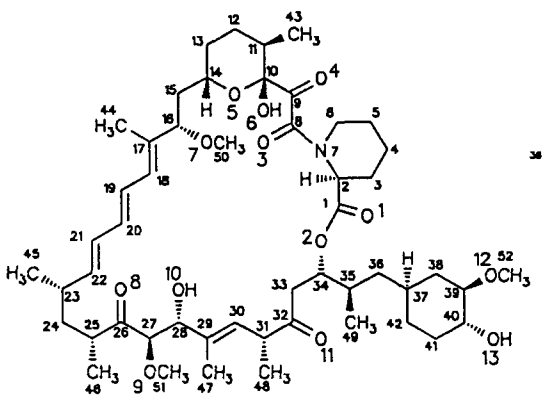

Rapamycin[a)]

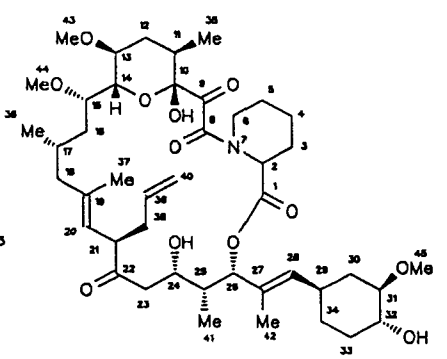

FK506

[a)] The numbering of atoms follows the rules for numbering of the *Cambridge Structure Data Bank:* first numbering of the main chain, then the Me groups.

Rapamycin binds to the same peptidyl-prolyl *cis-trans* isomerase FKBP [5] [6] as the structurally related immunosuppressant FK506. Recently, the structure of FKBP [7–9] and FK506 [6] [10] [11] as well as of their complex [9] was reported. Although the binding region (including C(1) to C(12) and C(31) to C(42)) of rapamycin and FK506 is almost

identical [2], the biological activity of the immunosuppressants is different: Rapamycin affects the lymphokine-receptor pathway at a later stage in the immunoresponse than FK506 which inhibits the signal-transduction pathway of the T-cell-receptor signal, whereas rapamycin hampers the activation of T-cell proliferation and differentiation by the interaction of interleucin II with its receptor [2]. This difference in activity is attributed to the differing structure of the rest of the molecule, the so-called activity domain, *i.e.* the region of C(13) to C(30).

FK506 exists in $CDCl_3$ solution as an equilibrium of two conformations about the amide bond, slowly interconverting on the NMR time scale (with respect to chemical shifts). The major *cis*-conformation is identical to the structure in the crystal; however, FK506 bound to FKBP corresponds to the minor *trans*-rotamer.

A drastic conformational change is also observed for the immunosuppressant cyclosporin A when bound [12]: whereas in less polar organic solvents and in the crystal, one conformation dominates, which exhibits one *cis* peptide bond about MeLeu^9 and MeLeu^{10}, the cyclophilin-bound conformation is all *trans*, partly similar to the conformation of the LiCl complex in THF solution [13]. The same overall structure is also found for CsA when bound to the Fab fragment of an immunoglobulin [14]. In polar solvents like MeOH and DMSO, a mixture of slowly interconverting conformers is observed.

Rapamycin exists in $CDCl_3$ solution as a mixture of 80% *trans*- and 20% *cis*-rotamer about the peptide bond. However, in DMSO, the *trans*-conformer is present in an amount of *ca.* 90%, which according to previous studies [15] is the same rotamer as found in the crystal. The assignment of the minor isomer as the *cis*-conformation has not been firmly established until now. Here we report the conformational analysis of the major conformation of rapamycin in DMSO by NMR spectroscopy and restrained molecular dynamics (MD) *in vacuo* and in DMSO. The solubility of rapamycin in H_2O is too low for NMR measurements (similar in this regard to FK506 and cyclosporin A).

Results and Discussion. – *Nuclear Magnetic Resonance.* All of the ^{1}H- and ^{13}C-NMR signals are assigned by a combination of 2D NMR techniques[1]) including TOCSY [16]. E.COSY [17], ROESY [18], NOESY [19], HMQC [20], and a modified HMBC [21]. The latter experiments combined with a *z*-filtered TOCSY [21] [22][2]) is applied to determine heteronuclear long-range coupling constants. All chemical shift values are listed in *Table 1*. Two sets of resonances are observed (ratio 9:1). Only the major isomer can be assigned. There is no evidence of chemical exchange (*i.e.* exchange peaks in the ROESY or NOESY spectra). Therefore, the minor resonances could arise from impurities or chemical degradation.

The assignment starts with the identification of six separated ^{1}H spin systems interrupted by quaternary C-atoms (CH_2(2) to CH_2(6), CH(43) to H–C(16), H–C(18) to CH_3(46), H–C(27) to OH(10), H–C(30) to CH_3(48), and CH_2(33) to CH_2(42)) from the TOCSY spectrum. In the first step, the small spin system H–C(27) to OH(10) is recognized by the only three coupled signals exhibiting low-field shifts caused by O-substitution. The

[1]) All NMR spectra were recorded at 300 K on an *AMX-600* spectrometer equipped with *Aspect-X32* and *Aspect-3001* computers. A sample of rapamycin (18 mg) was dissolved in 0.5 ml of (D_6)DMSO to give a final concentration of *ca.* 40 mM.

[2]) The pulse sequence for *AMX* spectrometers was programmed by *P. Schmieder*.

Table 1. *Assignment of ^{13}C- and ^{1}H-NMR Chemical Shifts in (D_6)DMSO*

Atom(s)	δ(H)	δ(C)	Atom(s)	δ(H)	δ(C)
C(1)		166.97	CH(27)	3.92	85.52
CH(2)	4.92	50.74	CH(28)	3.99	75.72
CH_2(3)	1.56(H_{ax}), 2.08(H_{eq})	26.41	C(29)		137.12
CH_2(4)	1.38(H_{ax}), 1.65(H_{eq})	20.35	CH(30)	5.08	124.93
CH_2(5)	1.26(H_{ax}), 1.55(H_{eq})	24.45	CH(31)	3.27	45.19
CH_2(6)	3.15(H_{ax}), 3.41(H_{eq})	43.48	C(32)		207.52
OH(6)	6.43		CH_2(33)	2.37($H_{pro\text{-}S}$), 2.72($H_{pro\text{-}R}$)	39.94
C(8)		169.18	CH(34)	4.97	73.56
C(9)		198.87	CH(35)	1.66	33.35
C(10)		98.99	CH_2(36)	1.03, 0.94[a])	38.39
OH(10)	5.23		CH(37)	1.23	32.51
CH(11)	2.01	34.78	CH_2(38)	0.58(H_{ax}), 1.88(H_{eq})	35.43
CH_2(12)	0.83(H_{ax}), 1.51(H_{eq})	31.09	CH(39)	2.81	83.73
CH_2(13)	1.80(H_{eq}), 1.16(H_{ax})	29.61	CH(40)	3.16	73.21
CH(14)	3.99	66.19	CH_2(41)	1.73(H_{eq}), 1.15(H_{ax})	32.88
CH_2(15)	1.24($H_{pro\text{-}R}$), 1.83($H_{pro\text{-}S}$)	40.13	CH_2(42)	1.52, 1.52[b])	26.22
CH(16)	3.61	82.24	CH_3(43)	0.72	15.52
C(17)		137.84	CH_3(44)	1.62	10.45
CH(18)	6.10	126.97	CH_3(45)	0.97	21.63
CH(19)	6.39	127.02	CH_3(46)	0.82	13.39
CH(20)	6.21	132.30	CH_3(47)	1.73	13.39
CH(21)	6.12	130.41	CH_3(48)	0.86	15.56
CH(22)	5.45	139.28	CH_3(49)	0.77	14.71
CH(23)	2.20	35.18	CH_3(50)	3.04	55.44
CH_2(24)	1.02 ($H_{pro\text{-}S}$), 1.39($H_{pro\text{-}R}$)	39.62	CH_3(51)	3.15	56.92
CH(25)	2.39	39.57	CH_3(52)	3.31	56.73
C(26)		210.49			

[a]) The diastereotopic assignment of the 2 H–C(36) was not accomplished in this work because no unambiguous differentiation could be done with the few available NOE's including this group.

[b]) Signals are nearly identical.

second short spin system, *H*–C(30) to CH_3(48), includes one Me group and one olefinic proton. On the other hand, the longest spin system in the molecule, from CH_2(33) to CH_2(42) including the Me protons at C(49), is identified both by the large number of protons involved and the two low-field shifted signals of *H*–C(39) and *H*–C(40). Five olefinic signals can be observed in the fragment starting at *H*–C(18) and extending to CH_3(46). At this stage of the assignment procedure, there remain two unidentified ^{1}H systems, the tetrahydropyran and the piperidine system. The signals of the tetrahydropyran moiety are identified by the presence of a Me group (CH_3(43)) which is absent in the piperidine system. The signals of all protonated C-atoms are assigned with the help of the HMQC spectrum, whereas the signals of all quaternary C-atoms, with the exception of C(47) and C(44), can be unambiguously identified by appropriate long-range correlations in the HMBC experiment. NOE signals between CH_3(44)/*H*–C(18), CH_3(44)/*H*–C(19), CH_3(47)/*H*–C(27), and CH_3(47)/*H*–C(28) allow the assignment of the remaining two Me groups.

To illustrate the assignment, a detailed description of the assignment procedure is given for the molecular fragment C(17) to C(26). First a cross-section through the *z*-filtered TOCSY spectrum at $F_1 = 2.20$ ppm (*H*–C(23)) shows all coupled protons from *H*–C(18) to *H*–C(25), including CH_3(45) and CH_3(46) (*Fig. 1*). The *z*-filtered experiment is used to determine coupling constants (see below). Of course, the same result may be obtained with a standard TOCSY experiment, without a *z*-filter.

In the low-field region of the E. COSY spectrum (not shown), the signal identified as *H*–C(18) at 6.10 ppm has only one neighbour. The further step-by-step connectivity along the olefinic moiety leads directly to *H*–C(23). Arising from *H*–C(23), there are two cross-peaks, which show connectivities both to CH_3(45) and $H_{pro\text{-}R}$–C(24).

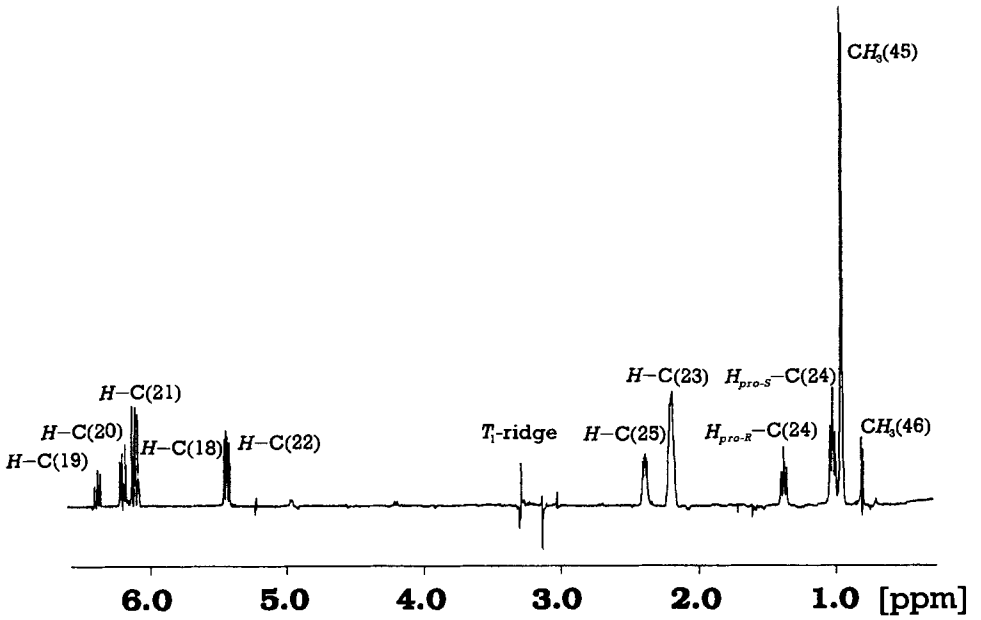

Fig. 1. *Cross-section through the z-filtered TOCSY spectrum illustrating the connectivity of all protons from* H–*C(18) to* H–*C(25) including both Me groups*

Because cross-peak intensities depend on homonuclear coupling constants, an expected third cross-peak is missing due to a small coupling constant between H–C(23) and $H_{pro\text{-}S}$–C(24). The remaining connectivity may be easily obtained starting from $H_{pro\text{-}R}$–C(24). Of course, in the case of the diastereotopic protons $H_{pro\text{-}S}$–C(24) and $H_{pro\text{-}R}$–C(24), there are two correlations in the HMQC spectrum.

As a last step, the assignment of C(26) is possible by a long-range correlation between C(26) and $H_{pro\text{-}R}$–C(24) (not shown). Unfortunately, there is no correlation in the HMBC spectrum which includes C(17). Nevertheless, the signal of this atom may be obtained unambiguously by the process of elimination. There are only two quaternary olefinic C-atoms in rapamycin. C(29) can be recognized using two correlations to H–C(28) and H–C(27), so the remaining atom must be C(17).

For the diastereospecific assignment of the methylene protons, a combination of homonuclear ^{1}H-NMR coupling constants and heteronuclear long-range coupling constants ^3J(C,H) is used. Two methods exist to measure the latter, even in the case of low concentration and severe spectral overlap; the method of *Titman et al.* [21] and HETLOC [23]. We decided to use the former method to measure coupling constants since the quaternary C-atoms C(17) and C(26) are important for the assignment of the corresponding protons $H_{pro\text{-}R}$–C(15)/$H_{pro\text{-}R}$–C(15) and $H_{pro\text{-}S}$–C(24)/$H_{pro\text{-}S}$–C(24). A disadvantage of this method, however, is the low intensity of cross-peaks and their strong dependence on heteronuclear coupling constants. It is impossible to get all necessary coupling constants in one experiment with reasonable intensity. A good signal/noise ratio is essential for the fitting procedure as described in more detail in *Fig. 2*.

To account for the different coupling constants, two HMBC measurements with delays of 55 and 80 ms, respectively, are used to yield the coupling constants given in *Table 2*[3]). With these values, an unambiguous assignment of the pairs $H_{pro\text{-}R}$–C(15)/$H_{pro\text{-}S}$–C(15), $H_{pro\text{-}R}$–C(24)/$H_{pro\text{-}S}$–C(24) and $H_{pro\text{-}R}$–C(33)/$H_{pro\text{-}S}$–C(33) is possible. No assignment is possible in the case of $H_{pro\text{-}R}$–C(36)/$H_{pro\text{-}S}$–C(36) because the difference in the coupling constants from the neighbour protons is too small for a reliable determination of the absolute configuration. An example of the diastereotopic assignment is given in *Fig. 3*.

[3]) All computation was carried out by self-modified FELIX vers. 1.0; *Hare Research*, Woodinville, Washington.

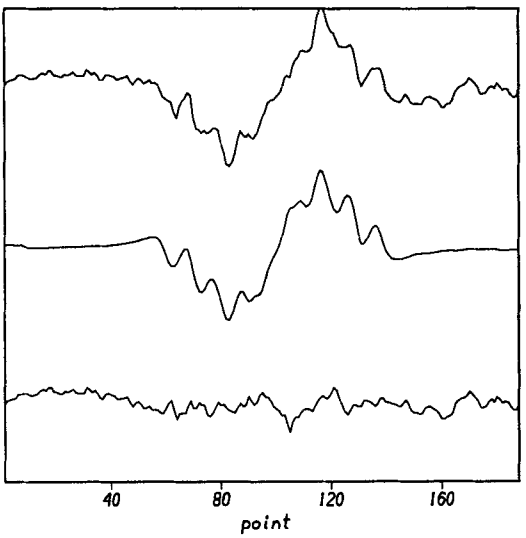

Fig. 2. *Illustration of the extraction of heteronuclear long-range coupling constants.* Top trace: Section through the cross-peak between C(13) and $H_{pro\text{-}S}$–C(15). Middle trace: Simulated signal arising from the $H_{pro\text{-}S}$–C(15) peak in the *z*-TOCSY spectrum. The simulation starts from the pure-phase *multiplet* of $H_{pro\text{-}S}$–C(15). From this a phase-shifted *multiplets* is constructed. Two of these modified *multiplets*, which are shifted by $J(H\text{–}C(15),C(13))$, are subtracted. Bottom trace: difference between the two upper traces.

Table 2. *Vicinal Coupling Constants as Derived from E.COSY and the Combination of HMBC and z-Filtered TOCSY and Additionally, in the Case of Crowded Coupling Patterns, the Sum of All Coupling Constants from a Given Proton to all Geminal and Vicinal Protons* H_x

Atoms	Coupling constant [Hz]	Dihedral angle [°]	Atoms	Coupling constant [Hz]	Dihedral angle [°]
H–C(2), H_{ax}–C(3)	6	46	H–C(22), H–C(23)	9.6	
H–C(2), H_{eq}–C(3)	2.9	67	H–C(23), H–C(24)	3.1	62
H_{ax}–C(3), H_{ax}–C(4)	13.3	180	H–C(23), H–C(24)	11.6	167
H_{ax}–C(3), H_{eq}–C(4)	3.4	60	H–C(23), H–C(45)	6.5	
H_{eq}–C(3), H_{ax}–C(4)	6.8	40	$H_{pro\text{-}R}$–C(24), H–C(25)	2.7	65
H_{ax}–C(4), H_{ax}–C(5)	12.8	180	$H_{pro\text{-}S}$–C(24), H–C(25)	11.1	162
H_{eq}–C(4), H_{ax}–C(5)	3.5	59	H–C(25), CH_3(46)	6.5	
H_{ax}–C(5), H_{ax}–C(6)	12.6	180	H–C(27), H–C(28)	4.7	56
H_{ax}–C(5), H_{eq}–C(6)	4.5	55	H–C(28), OH(10)	4.5	
H_{eq}–C(5), H_{ax}–C(6)	3.5	62	H–C(30), H–C(31)	10.1	
H_{eq}–C(5), H_{eq}–C(6)	3.5	62	H–C(31), CH_3(48)	6.5	
$\Sigma\lvert J(H_{ax}\text{–C(6)}, H_x)\rvert$	46.8		$H_{pro\text{-}R}$–C(33), H–C(34)	2.8	71
H–C(11), CH_3(43)	6.7		$H_{pro\text{-}S}$–C(33), H–C(34)	8.7	156
$\Sigma\lvert J(H_{ax}\text{–C(12)}, H_x)\rvert$	42.2		H–C(34), H–C(35)	4.5	53 or 137
$\Sigma\lvert J(H_{eq}\text{–C(12)}, H_x)\rvert$	24.6		H–C(35), H–C(36)	4.9	127 or 51
$\Sigma\lvert J(H_{ax}\text{–C(13)}, H_x)\rvert$	41.7		H–C(35), H'–C(36′)	9.1	24 or 149
$\Sigma\lvert J(H_{eq}\text{–C(13)}, H_x)\rvert$	29.1		H–C(35), CH_3 (49)	4.6	
H–C(14), $H_{pro\text{-}R}$–C(15)	10.0	164	H–C(36), H–C(37)	8.5	
H–C(14), $H_{pro\text{-}S}$–C(15)	3.6	65	H–C(36), H–C(37)	5.4	
$\Sigma\lvert J(H\text{–C(14)}, H_x)\rvert$	27.5		H_{ax}–C(38), H–C(39)	11.1	175

Table 2 (cont.)

Atoms	Coupling constant [Hz]	Dihedral angle [°]	Atoms	Coupling constant [Hz]	Dihedral angle [°]
$H_{pro\text{-}R}$–C(15), H–C(16)	2.3	75	H_{eq}–C(38), H–C(39)	4.4	60
$H_{pro\text{-}S}$–C(15), H–C(16)	11.6	180	H–C(39), H–C(40)	8.6	180
H–C(18), H–C(19)	11.2		H–C(40), H_{ax}–C(41)	11.1	174
H–C(19), H–C(20)	14.6		H–C(40), H_{eq}–C(41)	4.6	58
H–C(29), H–C(21)	10.6		$\Sigma\|J(H_{ax}\text{–C(41)}, H_x)\|$	41.6	
H–C(21), H–C(22)	14.9		$\Sigma\|J(H_{eq}\text{–C(41)}, H_x)\|$	21	
H–C(2), C(4)	± 6.9		H–C(30), C(28)	± 7.8	
H–C(2), C(6)	± 4.9		H–C(39), C(47)	± 5.5	
CH(13), C(11)	± 8.2		$H_{pro\text{-}R}$–C(33), C(35)	± 2.6	
$H_{pro\text{-}S}$–C(15), C(13)	± 6.6		$H_{pro\text{-}S}$–C(33), C(35)	± 2.7	
H–C(16), C(18)	± 4.7		CH_3(43), C(10)	± 2.4	
H–C(16), C(44)	± 3.9		CH_3(46), C(26)	± 4.4	
H–C(16), C(50)	± 3.1		CH_3(48), C(30)	± 4.9	
$H_{pro\text{-}R}$–C(24), C(22)	± 3.7		CH_3(48), C(32)	± 4.4	
$H_{pro\text{-}R}$–C(24), C(26)	± 2.9				

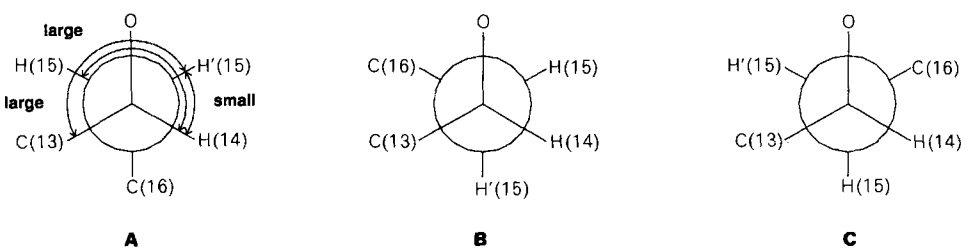

Fig. 3. *Assignment of the conformation between C(14) and C(15).* According to the coupling constants (*Table 2*), one H–C(15) is antiperiplanar to H–C(14), the other H–C(15) synclinal to H–C(14); this condition is fulfilled in the rotamers **A** and **C**. Furthermore, the large heteronuclear coupling constant J(H–C(15),C(13)) indicates an antiperiplanar position, and the same proton (= H'(15)) is synclinal to H–C(14). This is only fulfilled in conformation **A**. In conformation **C**, no large vicinal heteronuclear coupling constant can be observed. The conformation between C(15) and C(16) is then unambiguously determined by the antiperiplanar conformation of H–C(16) and $H_{pro\text{-}S}$–C(15).

The computation of dihedral angles from coupling constants is done with a modified *Karplus* equation [24] [25] (*Table 2*). Even at 600 MHz, it is almost impossible to completely resolve a few very crowded *m*'s of the six-membered-ring protons. In these cases, the frequency difference between the two limiting lines of the *m*, which represents the sum of all homonuclear coupling constants to the neighbour protons are used to differentiate between the axial or equatorial position of the corresponding proton [26].

A total of 66 distance restraints derived from NOESY spectra with the two-spin approximation and calibrated using geminal protons (assumed distance of 1.78 Å) are applied with a skewed biharmonic constraining function in the MD simulations.

MD Calculations. Both *in vacuo* and solvent simulations (DMSO) are carried out in this study (see *Exper. Part*). The *in vacuo* simulations should allow greater conformational mobility, large structural changes are not possible in solvent simulations of reason-

able duration (100 ps). The solvent simulations are then used to try to mimic as best as possible the conditions in which the NMR measurements are carried out.

The root-mean-square (r.m.s.) difference of all atoms (without the flexible side chain containing the cyclohexane ring) between the X-ray structure and the calculated structure *in vacuo* (**I** (vac.)) is 1.508 Å and 0.928 Å between **I** (vac.) and **II** (vac.). Hence, the final structure obtained from the *in vacuo* calculations is independent from the starting conformation. However, *in vacuo* calculations were shown to give rise to artifacts even when experimental constraints are used [27]. In the solvent simulations, again very similar structures are obtained in the case of **I** (DMSO) and **II** (DMSO) using the different starting structures mentioned above. In the minimized structures, nearly identical distance violation averages of 0.27 and 0.26 Å, resp., are observed (including all experimentally derived distances, except those containing Me groups, geminal protons, or the protons at C(36) not diastereotopically assigned).

The effective average distances $r_{eff} = \langle r^{-3} \rangle^{1/3}$ [28] are given in *Table 3* for **II** (DMSO), taking into account the nonlinear distance dependence of the NOE. An average violation of 0.17 Å is observed between these and the experimental distances (with the same exceptions as above).

Stereoplots of the minimized average structures **I** (DMSO) and **II** (DMSO) are shown in *Figs. 4* and *5*; distances and dihedral angles are summarized in *Tables 3* and *4*, respectively.

As expected, the cyclohexyl-substituted side chain cannot be localized with the experimental distances. Both simulations in DMSO yield different orientations of this group depending on the initial position. However, this is to be expected since there are only 8 restraints to force this group into a distinct orientation (see torsions C(35)–C(36) and

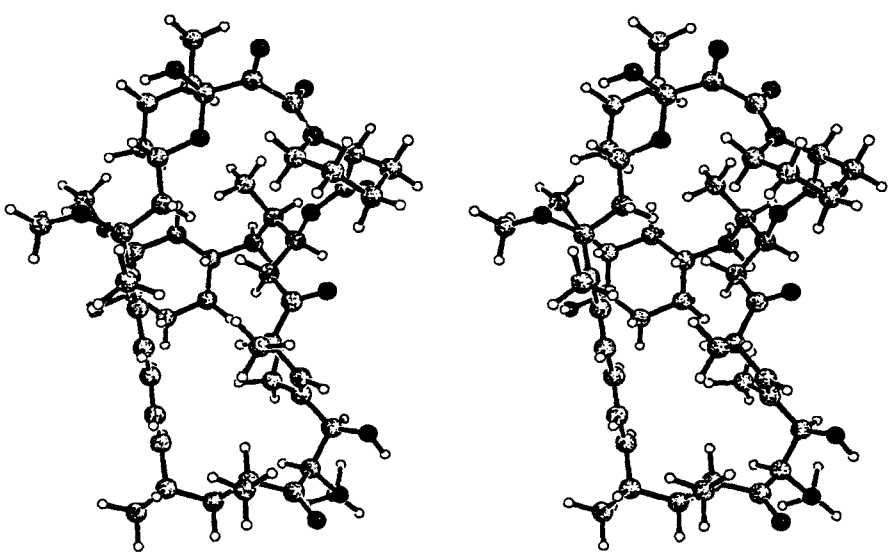

Fig. 4. *Stereostructure of the conformation* **I** *(DMSO) of rapamycin obtained by averaging a trajectory of 50 ps of molecular dynamics and energy minimization*

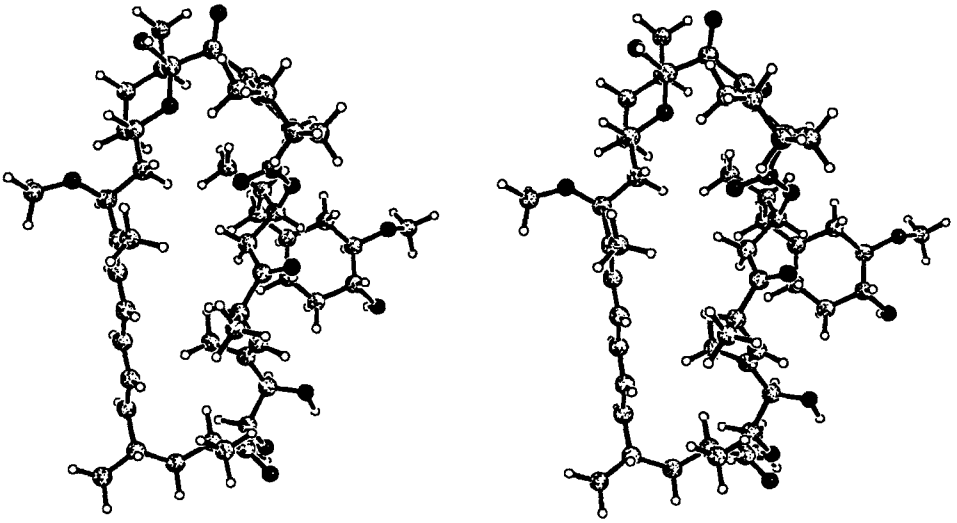

Fig. 5. *Minimized stereostructure of the conformation* **II** *(DMSO) of rapamycin obtained by averaging a trajectory of 50 ps of molecular dynamics which started from a manually built 'open' structure*

Table 3. *Comparison of the Proton Distance Restraints Derived from NOESY Experiments*[a]) *with the Energy-Minimized Results of the MD calculations.* For **II** (DMSO), the average values are also given.

Atoms		$r(H,H)_{exp.,\,NOE}$	$r(H,H)_{calc.}$		
			I (DMSO), minimized	**II** (DMSO), minimized	**II** (DMSO), averaged[b])
H–C(2)	H_{ax}–C(3)	2.44	2.30	2.32	2.32
H–C(2)	H_{eq}–C(3)	2.54	2.55	2.55	2.55
H_{ax}–C(3)	H_{eq}–C(3)	1.78	1.75	1.75	
H_{ax}–C(3)	H_{eq}–C(4)	2.79	2.48	2.48	2.56
H_{eq}–C(3)	H_{eq}–C(4)	2.35	2.52	2.53	2.50
H_{ax}–C(5)	H_{eq}–C(6)	2.52	2.42	2.42	2.43
H_{eq}–C(5)	H_{eq}–C(6)	2.49	2.51	2.51	2.51
H_{ax}–C(6)	H_{eq}–C(6)	1.76	1.75	1.76	
O*H*(10)	*H*–C(28)	2.46	2.25	2.25	2.32
H–C(11)	H_{eq}–C(12)	2.55	2.48	2.48	2.45
H–C(11)	H_{ax}–C(13)	2.78	2.78	2.70	2.70
H–C(11)	C(43)	2.19	2.15	2.15	
H_{eq}–C(12)	H_{eq}–C(13)	2.38	2.54	2.52	2.51
H_{eq}–C(12)	C(43)	2.32	2.78	2.77	
H_{eq}–C(13)	C(50)	3.70	3.38	3.74	
H–C(14)	$H_{pro\text{-}R}$–C(15)	2.72	3.06	3.08	2.99
H–C(14)	$H_{pro\text{-}S}$–C(15)	2.21	2.41	2.51	2.36
H–C(14)	*H*–C(16)	3.10	3.42	3.19	3.17
$H_{pro\text{-}R}$–C(15)	*H*–C(16)	2.53	2.40	2.47	2.46
H–C(16)	H_{ax}–C(13)	2.85	2.86	3.03	2.84
H–C(16)	*H*–C(18)	2.15	2.26	2.23	2.18
H–C(16)	C(50)	2.59	2.57	2.55	
H–C(18)	C(44)	3.72	3.53	3.53	
H–C(18)	C(50)	3.23	4.02	3.84	
H–C(19)	C(44)	2.30	2.64	2.66	
H–C(20)	*H*–C(22)	2.46	2.41	2.40	2.47

Table 3 (cont.)

Atoms		$r(H,H)_{exp.,\ NOE}$	$r(H,H)_{calc.}$		
			I (DMSO), minimized	II (DMSO), minimized	II (DMSO), averaged[b])
H–C(20)	C(47)	3.23	4.04	3.74	
H–C(21)	H–C(23)	2.38	2.36	2.38	2.38
H–C(21)	H–C(25)	3.13	3.16	3.03	3.11
H–C(21)	C(46)	2.64	3.43	3.52	
H–C(22)	H–C(23)	2.98	3.12	3.12	3.03
H–C(22)	$H_{pro\text{-}S}$–C(24)	2.71	3.93	3.92	3.42
H–C(22)	H–C(25)	3.09	3.21	3.26	3.21
H–C(22)	C(45)	2.69	2.76	2.75	
H–C(23)	$H_{pro\text{-}R}$–C(24)	3.13	3.07	3.08	3.13
H–C(23)	$H_{pro\text{-}S}$–C(24)	2.60	2.50	2.52	2.54
H–C(23)	C(45)	2.34	2.14	2.14	
H–C(23)	C(46)	2.45	2.89	2.90	
$H_{pro\text{-}R}$–C(24)	H–C(25)	2.78	2.54	2.56	2.53
$H_{pro\text{-}R}$–C(24)	H–C(27)	2.59	2.38	2.43	2.65
$H_{pro\text{-}S}$–C(24)	$H_{pro\text{-}R}$–C(24)	1.84	1.75	1.75	
$H_{pro\text{-}S}$–C(24)	H–C(25)	2.88	3.07	3.07	3.08
H–C(25)	H–C(27)	2.72	2.68	2.62	2.67
H–C(25)	H–C(28)	2.93	4.07	4.05	3.55
H–C(25)	H–C(30)	3.29	3.23	3.28	3.52
H–C(25)	C(46)	2.30	2.13	2.13	
H–C(27)	C(47)	2.36	2.87	2.86	
H–C(27)	C(51)	2.68	2.53	2.53	
H–C(28)	H–C(30)	2.56	3.50	3.51	2.83
H–C(28)	C(47)	2.71	2.69	2.69	
H–C(30)	H–C(31)	2.83	3.06	3.09	3.02
H–C(30)	C(48)	2.66	2.68	2.75	
H–C(31)	$H_{pro\text{-}R}$–C(33)	2.80	2.44	2.59	2.83
H–C(31)	$H_{pro\text{-}S}$–C(33)	2.79	2.84	2.71	2.63
$H_{pro\text{-}R}$–C(33)	H–C(34)	2.64	2.49	2.46	2.42
$H_{pro\text{-}R}$–C(33)	H–C(36)	2.78	2.65	3.82	3.60
$H_{pro\text{-}R}$–C(33)	H–C(36)	2.78	3.87	2.36	2.45
$H_{pro\text{-}R}$–C(33)	H_{eq}–C(41)	3.02	4.47	4.44	3.69
$H_{pro\text{-}R}$–C(33)	C(49)	2.81	3.74	3.39	
$H_{pro\text{-}S}$–C(33)	$H_{pro\text{-}R}$–C(33)	1.84	1.76	1.75	
$H_{pro\text{-}S}$–C(33)	H–C(34)	3.05	3.07	3.07	3.08
H–C(34)	H–C(35)	2.53	2.34	2.43	2.34
H–C(34)	H–C(36)	2.90	2.61	3.72	3.28
H–C(34)	H–C(37)	3.06	3.85	3.96	3.62
H–C(34)	C(49)	3.00	3.50	3.48	
H–C(37)	H–C(39)	2.93	2.58	2.64	2.77
H–C(37)	H_{ax}–C(41)	2.83	2.57	2.69	2.88
H_{ax}–C(38)	H_{eq}–C(38)	1.97	1.76	1.76	
H_{ax}–C(38)	H–C(39)	3.30	3.10	3.08	3.12
H_{eq}–C(38)	H–C(39)	2.68	2.50	2.47	2.55
H_{ax}–C(38)	H–C(40)	2.58	2.73	2.71	2.63
H_{eq}–C(38)	C(52)	3.57	3.11	3.62	
H–C(40)	H_{eq}–C(41)	2.90	2.51	2.49	2.60

[a]) The distance between H_{ax}– and H_{eq}–C(3) was used for calibration, assuming a distance of 1.78 Å.

[b]) All distances to Me protons and between geminal protons were not used in the averaging.

Table 4. *Dihedral Angles* [°] *of Rapamycin: X-Ray Structure and Averages and Standard Deviations of the MD Calculations in DMSO.* **I** (DMSO) started from the *in vacuo* structure derived from the crystal structure, **II** (DMSO) from the 'open' structure.

Torsion	X-Ray	**I** (DMSO)		**II** (DMSO)	
		Average MD	Standard deviation	Average MD	Standard deviation
C(1)–C(2)–C(3)–C(4)	–82	–82	6.8	–81	6.5
C(2)–C(3)–C(4)–C(5)	–55	–58	5.3	–56	5.5
C(3)–C(4)–C(5)–C(6)	58	55	5.4	55	5.4
C(4)–C(5)–C(6)–N(7)	–52	–47	7.8	–48	6.7
C(5)–C(6)–N(7)–C(2)	42	41	9.7	43	8.9
C(6)–N(7)–C(2)–C(3)	–40	–42	8.2	–43	8.3
C(2)–N(7)–C(8)–C(9)	–170	–177	4.7	177	7.7
N(7)–C(8)–C(9)–C(10)	–105	–88	6.2	–88	6.0
C(8)–C(9)–C(10)–C(11)	–51	–50	12.6	–66	19.7
C(9)–C(10)–C(11)–C(12)	166	165	5.6	166	6.0
C(10)–C(11)–C(12)–C(13)	–52	–52	5.3	–52	4.6
C(11)–C(12)–C(13)–C(14)	52	54	5.6	54	4.8
C(12)–C(13)–C(14)–C(15)	–174	–173	6.3	–172	5.7
C(13)–C(14)–C(15)–C(16)	–67	–56	6.9	–57	7.3
C(14)–C(15)–C(16)–C(17)	173	178	7.5	178	8.0
C(15)–C(16)–C(17)–C(18)	–116	–120	7.1	–121	6.7
C(16)–C(17)–C(18)–C(19)	174	179	7.1	–177	7.1
C(17)–C(18)–C(19)–C(20)	176	178	7.0	179	6.8
C(18)–C(19)–C(20)–C(21)	171	174	7.1	–172	7.8
C(19)–C(20)–C(21)–C(22)	–173	177	6.1	176	6.0
C(20)–C(21)–C(22)–C(23)	168	–179	5.8	–178	6.6
C(21)–C(22)–C(23)–C(24)	–112	–108	4.6	–108	4.5
C(22)–C(23)–C(24)–C(25)	64	72	4.5	73	4.6
C(23)–C(24)–C(25)–C(26)	–165	–176	4.5	177	4.8
C(24)–C(25)–C(26)–C(27)	97	95	6.3	96	6.4
C(25)–C(26)–C(27)–C(28)	84	*51*[a])	7.2	*56*[a])	8.5
C(26)–C(27)–C(28)–C(29)	–80	–91	6.0	–88	7.3
C(27)–C(28)–C(29)–C(30)	122	*165*[a])	6.6	*156*[a])	10.1
C(28)–C(29)–C(30)–C(31)	173	168	7.1	175	7.6
C(29)–C(30)–C(31)–C(32)	–113	*–89*[a])	18.6	–96	13.1
C(30)–C(31)–C(32)–C(33)	77	*147*[a])	15.6	*118*[a])	17.2
C(31)–C(32)–C(33)–C(34)	–156	*161*[a])	13.3	*175*[a])	11.8
C(32)–C(33)–C(34)–O(2)	–89	–74	8.0	*–62*[a])	8.3
C(33)–C(34)–O(2)–C(1)	155	141	26.3	*46*[a])	95.2
C(34)–O(2)–C(1)–C(2)	–173	–178	12.1	–165	14.4
O(1)–C(1)–C(2)–C(3)	–59	–65	30.7	*17*[a])	82.7
C(9)–C(10)–O(5)–C(14)	–180	–175	6.3	–175	6.7
C(10)–O(5)–C(14)–C(15)	–176	–180	6.8	–179	7.3
C(33)–C(34)–C(35)–C(36)	–73	–65	7.7	–65	4.8
C(34)–C(35)–C(36)–C(37)	–57	*68*[a])	9.8	–45	6.1
C(35)–C(36)–C(37)–C(38)	–177	*131*[a])	13.6	*–49*[a])	6.1
C(36)–C(37)–C(38)–C(39)	177	177	5.5	177	8.0
C(37)–C(38)–C(39)–C(40)	–58	–51	4.3	–52	5.1
C(38)–C(39)–C(40)–C(41)	61	52	4.6	57	6.4
C(39)–C(40)–C(41)–C(42)	–61	–59	5.1	–53	6.1
C(40)–C(41)–C(42)–C(37)	59	65	3.5	45	9.9
C(41)–C(42)–C(37)–C(36)	–175	165	4.7	–177	12.5

[a]) These values differ by more than 20° from the X-ray structure.

C(36)–C(37) in *Table 4*). A structure with an external orientation is favoured because of the absence of NOE's to the macrolid backbone.

The flexibility of the backbone of the macrolide is restricted by a number of stabilizing structural elements, *i.e.* the stiff conjugated triene moiety, a further isolated double bond, the tetrahydropyran system and the piperidin-1,2-diyl moiety. This is reflected in the standard deviations of the torsion values in *Table 4*.

Lastly the calculations in the DMSO environment lead to structures of the ring which are very similar to the X-ray structure. The r.m.s. difference of the coordinates of all atoms (except for the cyclohexyl-substituted side chain) between the structures in DMSO and the crystal structure is 1.15 Å for **I** (DMSO) and 0.96 Å for **II** (DMSO).

Compared to the crystal structure, the lactone group has changed its orientation in **II** (DMSO), affecting only the C(34)–O(2) and C(1)–C(2) torsions which also show large correlated angle fluctuations in the simulations. However, lactones normally favour a planar horseshoe-like orientation of the COOCH group [29], which also can be expected for H–C(34)–O(2)–C(1)–O(1). Such an arrangement is found for **I** (DMSO).

Further structural changes occur in the torsions of the backbone in the region C(26)–C(33) (see *Table 4*, values in italics). Here higher torsional fluctuations during the simulations are obtained, especially for the bonds C(30)–C(31), C(31)–C(32), and C(32)–C(33) which are localized in the region around the connection of the exocyclic side chain to the backbone. The latter motions are not correlated with structural changes of the ester group.

The amide bond of the major isomer of rapamycin in DMSO solution is *trans*-configurated. There is no unambiguous proof that the second isomer (*ca.* 10%) is the corresponding *cis*-conformer. However, the *trans*-configuration can be proven by comparison of a few characteristic chemical shifts (δ(C(2)), δ(*H*–C(2)), δ(C(6)), δ(H_{ax}–C(6)), and δ(H_{eq}–C(6)) with the corresponding values of FK506 (see *Table 5*) [11].

Table 5. *Characteristic Chemical Shifts in Rapamycin and FK506* [11]

	Rapamycin δ ((D$_6$)DMSO)	*cis*-FK506 δ ($CDCl_3$)	*trans*-FK506 δ ($CDCl_3$)
C(2)	50.74	56.55	52.69
H–C(2)	4.91	4.53	4.94
C(6)	43.48	39.22	43.85
H_{ax}–C(6)	3.15	2.98	3.14
H_{eq}–C(6)	3.41	4.36	3.68

This was carried out previously with success: it was possible to predict the correct configuration of receptor-bound FK506 only based on the chemical shifts before it was completely solved [30].

A comparison of the binding regions [2] of rapamycin and of FK506 – which adopts both *cis*- and *trans*-configuration (ratio 2:1) with respect to the pseudo-peptide bond in $CDCl_3$ solution [10] – shows a good agreement of the conformations of the α-keto-piperidyl ring, the diketo group, and the carbonyl group of the lactone moiety in **I** (DMSO). The conformations of the here discussed immunosuppressants in different environments are summarized in *Table 6*.

Table 6. *Observable Conformers of the Immunosuppressants in Different Solvents, in the Crystal, and in the Receptor-Bound State*

	Solution $CDCl_3$	Solution DMSO	Crystal	Receptor-bound state
CsA	9,10-*cis*	> 7 conformers	9,10-*cis*	all-*trans*
FK506	*cis*/*trans* 2:1		*cis*	*trans*
Rapamycin	*cis*/*trans* 1:4	*cis*[a])/*trans* 1:10	*trans*	*trans*
CsA·*n* LiCl	all-*trans*[b])			

[a]) The minor conformation is assumed to be *cis*. [b]) In THF.

Conclusions. – The conformation of rapamycin in DMSO was derived using NOE data for distance determination. All ^{1}H- and ^{13}C-NMR shifts were assigned, and many homo- and heteronuclear coupling constants were extracted using recently developed NMR techniques. Both simulations in DMSO converged to a structure of rapamycin which shows no significant difference to the X-ray structure. This is in contrast to FK506 where great differences were observed.

Supplementary Material. – The coordinates of rapamycin after MD simulations (averaged and minimized) and a few useful PASCAL programs for the inspection of DISCOVER files are available from the authors upon request.

We gratefully acknowledge for financial support by the *Deutsche Forschungsgemeinschaft* and the *Fonds der Chemischen Industrie* as well as for a fellowship to *R. H.* by the *Alexander von Humboldt Stiftung*. We thank Prof. *J. Keeler* for the program to extract long-range coupling constants and his support in the implementation on our computers and *Dale F. Mierke* and *G. Gemmecker* for careful reading of the manuscript.

Experimental Part

Measurement Conditions. 1. *600-MHz NOESY Spectrum* (300 K): Sequence D_1–90°–t_1–90°–τ_{mix}–90°–t_2. Relaxation delay D_1 = 1 s, mixing time τ_{mix} = 100 ms, 90° pulse 13.9 μs, sweep width 3968 Hz in F_1 and F_2. 4 K points in t_2, 512 experiments in t_1, quadrature detection in both dimensions, zero filling up to 512 real points in F_1 and apodization with a $\pi/2$-shifted squared sine bell in both dimensions. The integration was carried out after baseplane correction.

2. *600-MHz E.COSY Spectrum* (300 K): Sequence D_1–90°–t_1–90°–90°–t_2. Relaxation delay D_1 = 0.8 s, 8 K data points in t_2, sweep width 3788 Hz in F_1 and F_2, 1024 experiments in t_1, quadrature detection in both dimensions, zero filling up to 4 K real points in F_1 and apodization with a $\pi/2$-shifted squared sine bell in both dimensions.

3. *600/150-MHz-Modified HMBC Spectrum* (300 K): Sequence D_1–90° (^{1}H)–Δ–90° (^{13}C)–$t_1/2$–180° (^{1}H)–$t_1/2$–180° (^{1}H)–90° (^{13}C)–t_2. Relaxation delay D_1 = 0.4 s, 90° pulse 12.9 μs for ^{1}H and 9.7 μs for ^{13}C, evolution delay Δ = 55 ms, 8 K data points in t_2, sweep width 3788 Hz in F_2 and 32113 Hz in F_1, 512 experiments in t_1, quadrature detection in both dimensions, zero filling up to 512 real points in F_1 and apodization with a $\pi/2$-shifted squared sine bell in both dimensions.

4. *600-MHz TOCSY with z-Filter* (300 K): Sequence D_1–90°–t_1–90°–Δ–DIPSI2–Δ–90°–t_2. In the DIPSI2 scheme, all given pulses are multiples of the 90° pulse: (3.555, 4.555, 3.222, 3.166, 0.333, 2.722, 4.166, 2.944, 4.111). Relaxation delay D_1 = 1.1 s, 90° pulse 12.9 μs for hard pulses and 26.5 μs as basis for DIPSI2, mixing time 50 ms, 8 different times from 0.5 ms to 20 ms for the filter delay Δ for each increment, 8 K data points in t_2, sweep width 3788 Hz in F_1 and F_2, 512 experiments in t_1, quadratur detection in both dimensions, zero filling up to 512 real points in F_1 and apodization with a $\pi/2$-shifted squared sine bell in both dimensions.

5. *600/150-MHz HMQC Spectrum with BIRD Presaturation* (300 K): Sequence D_1–90° (^{1}H)–Δ_1–180° (^{1}H)–180° (^{13}C)–Δ_1–90° (^{1}H)–Δ_2–90° (^{1}H)–Δ_1–90° (^{13}C)–$t_1/2$–180° (^{1}H)–$t_1/2$–90° (^{13}C)–Δ_1–t_2. Relaxation delay D_1 = 120 ms, presaturation delay Δ_2 = 230 ms, evolution delay Δ_1 = 3.45 ms, 90° pulse 13.9 μs for ^{1}H, 9.7 μs for ^{13}C hard pulses and 53.6 μs for ^{13}C GARP decoupling, 4 K data points in t_2, sweep width 3968 Hz in F_2 and 20833 Hz in F_1, 1024 experiments in t_1, quadratur detection in both dimensions, zero filling up to 1024 real points in F_1 and apodization with a $\pi/2$-shifted squared sine bell in both dimensions.

Molecular-Dynamics Simulations. The simulations [31] were performed with the DISCOVER software package (*Biosym Technologies*, San Diego) on *Silicon-Graphics-4D/240S* and *-4D/70GT* computers. The program INSIGHT II (*Biosym*) was used for interactive modeling and analysis. The crystal structure of rapamycin [15] served as the basis for generating the molecular topology and one of the starting structures for the simulations. Four MD simulations, two *in vacuo* and two in the same solvent as the NMR experiments (DMSO) were performed. Some force-field parameters concerning the energetic description of the tricarbonyl hemiacetal portion are undefined in the commonly utilized force fields and were introduced according to calculations of FK506 [11]. Other parameters which describe the triene moiety and carbonyl groups (except for the above mentioned tricarbonyl hemiacetal portion) were taken from closely related structural groups. Furthermore, the force-field parameters of DMSO were implemented as previously used [32].

Simulations in vacuo. Two different starting structures were used, the crystal structure for **I** (vac.) and a manually built 'open' structure for **II** (vac.).

I (vac.): The simulation started from the crystal structure of rapamycin using 66 experimental distances (*Table 3*; upper and lower distance bound set to ±0.3 Å of the calculated distances; united-atom model for Me groups with an upper-bound correction of +1.0 Å [33]). After calculating a simulated annealing procedure including a high-temperature phase (2 ps at 1000 K, 5 ps at 600 K) and then cooling to 300 K, the system was allowed to equilibrate for 43 ps. A further 50 ps of MD calculation at 300 K was used for analysis. From this, an average structure was calculated and energy-minimized with NOE restraints (united-atom model for Me groups; 0.3 Å correction to the upper bound [34]) to a final maximum derivative of 0.004 kJ·mol^{-1}·Å^{-1}. An intermediate structure of this minimization with a maximum derivative of 4.2 kJ·mol^{-1}·Å^{-1} served as starting structure for **I** (DMSO).

II (vac.): The simulation started from a manually built 'open' structure. In the high-temperature phase of the simulation, the force constants for the NOE restraints and force-field parameters were increased successively to their maximum value. In an MD simulation at 1000 K, the NOE distance forcing potentials were introduced step by step. The scaling of the distance restraint forcing potential was increased 32 times with an increment of 25%. The annealing procedure was carried out as in **I** (vac.). The average structure was energy minimized.

Further Refinement with Explicit DMSO Molecules. **I** (DMSO): The partially minimized structure described in **I** (vac.) was soaked with DMSO in a cubic solvent box (symmetry group $P1$, a = 36.28 Å, b = 32.28 Å, c = 32.24 Å, 255 DMSO molecules) applying periodic boundary conditions. Now the distance-restraining potential came into effect when the absolute deviations of the inter-proton distances from the experimental values exceeded 0.1 Å. An additional 0.2 Å was added to the upper distance bounds for all 20 Me groups in united-atom representation. The maximum force constant for the lower and upper distance restraints was 418 kJ·mol^{-1}·Å^{-2}. After an equilibration period of 70 ps, a trajectory of 50 ps was carried out for evaluation. The average structure was restrained-minimized by steepest descent followed by pseudo *Newton-Raphson* energy minimization leading to convergence at a maximum derivative of 0.04 kJ·mol^{-1}·Å^{1}.

II (DMSO): As in **II** (vac.), the random structure was taken as starting structure. Due to the different size of this conformation, a new box was designed (symmetry group $P1$, a = 34.85 Å, b = 31.38 Å, c = 31.37 Å, 227 DMSO molecules). The simulation began with a high-temperature phase (15 ps at 500 K). After a further period of 55 ps at 300 K for equilibration, a trajectory of 50 ps was recorded for evaluation. The average structure was minimized in the same manner as in **I** (DMSO).

REFERENCES

[1] C. Vécina, A. Kudelsdi, S. N. Sehgal, *J. Antibiot.* **1975,** *28,* 721; S. N. Sehgal, H. Baker, C. Vécina, *ibid.* **1975,** *28,* 727.

[2] S. L. Schreiber, *Science* **1991,** *251,* 283; M. K. Rosen, S. L. Schreiber, *Angew. Chem.* **1992,** *104,* 413.

[3] A. Rüegger, M. Kuhn, H. Licht, H. R. Loosli, R. Huguenin, C. Quiquerez, A. von Wartburg, *Helv. Chim. Acta* **1976,** *59,* 1075; T. J. Petcher, H. P. Weber, A. Rüegger, *ibid.* **1976,** *59,* 1480.

[4] H. Tanaka, A. Kuroda, H. Marusawa, H. Hatanaka, T. Kino, T. Goto, M. Hashimoto, *J. Am. Chem. Soc.* **1987,** *109,* 5031.

[5] M. W. Harding, A. Galat, D. E. Uehling, S. L. Schreiber, *Nature (London)* **1989,** *341,* 758.

[6] J. J. Siekierka, S. H. Y. Hung, M. Poe, C. S. Lim, N. H. Sigal, *Nature (London)* **1989,** *341,* 755.

[7] S. W. Michnick, M. K. Rosen, T. J. Wandless, M. Karplus, S. L. Schreiber, *Science* **1991,** *252,* 836.

[8] J. M. Moore, D. A. Peattle, M. J. Fitzgibbon, J. A. Thomson, *Nature (London)* **1991,** *351,* 248.

[9] G. D. van Duyne, R. F. Standaert, P. A. Karplus, S. L. Schreiber, J. Clardy, *Science* **1991,** *252,* 839.

[10] P. Karuso, H. Kessler, D. F. Mierke, *J. Am. Chem. Soc.* **1990,** *112,* 9434.

[11] D. F. Mierke, P. Schmieder, P. Karuso, H. Kessler, *Helv. Chim. Acta* **1991,** *74,* 1027.

[12] C. Weber, B. Wider, B. von Freyberg, R. Traber, W. Braun, H. Widmer, K. Wüthrich, *Biochemistry* **1991,** *30,* 6563; S. W. Fesik, T. R. Gampe, Jr., H. L. Eaton, G. Gemmecker, E. T. Olejniczak, P. Neri, T. F. Holzman, D. A. Egan, R. Edalji, R. Simmer, R. Helfrich, J. Hochlowski, M. Jackson, *Biochemistry* **1991,** *30,* 6574.

[13] M. Köck, H. Kessler, D. Seebach, A. Thaler, *J. Am. Chem. Soc.* **1992,** *114,* 2676.

[14] D. Altschuh, O. Vix, B. Rees, J.-C. Thierry, *Science* **1992,** *256,* 92.

[15] D. C. Swindells, P. S. White, J. A. Findlay, *Can J. Chem.* **1978,** *56,* 2491.

[16] L. Braunschweiler, R. R. Ernst, *J. Magn. Reson.* **1983,** *53,* 521; D. G. Davis, A. Bax, *J. Am. Chem. Soc.* **1985,** *107,* 2820.

[17] C. Griesinger, O. W. Sørensen, R. R. Ernst, *J. Am. Chem. Soc.* **1985,** *107,* 6394.

[18] A. A. Bothner-By, R. L. Stephens, J. Lee, C. D. Warren, R. W. Jeanloz, *J. Am. Chem. Soc.* **1984,** *106,* 811; A. Bax, D. G. Davis, *J. Magn. Reson.* **1985,** *65,* 355; H. Kessler, C. Griesinger, R. Kerssebaum, K. Wagner, R. R. Ernst, *J. Chem. Soc.* **1987,** *109,* 607.

[19] S. Macura, Y. Huang, D. Suter, R. R. Ernst, *J. Magn. Reson.* **1981,** *43,* 259.

[20] L. Mueller, *J. Am. Chem. Soc.* **1979,** *101,* 4481; A. Bax. S. Subramanian, *J. Magn. Reson.* **1986,** *67,* 565.

[21] J. J. Titman, D. Neuhaus, J. Keeler, *J. Magn. Reson.* **1989,** *85,* 111.

[22] M. Rance, *J. Magn. Reson.* **1987,** *74,* 557; A. J. Shaka, C. J. Lee, A. Pines, *J. Magn. Reson.* **1988,** *77,* 274.

[23] H. Kessler, P. Schmieder, *Biopolymers* **1991,** *31,* 621; see also G. T. Montelione, M. E. Winkler, P. Rauenbühler, G. Wagner, *J. Magn. Reson.* **1989,** *82,* 198.

[24] C. A. G. Haasnoot, F. A. A. M. de Leeuw, C. Altona, *Tetrahedron* **1980,** *36,* 2783.

[25] M. L. Huggins, *J. Am. Chem. Soc.* **1953,** *75,* 4123.

[26] H. Feltkamp, N. C. Franklin, *Angew. Chem.* **1965,** *77,* 798.

[27] M. Kurz, D. F. Mierke, H. Kessler, *Angew. Chem. Int. Ed.* **1992,** *31,* 210.

[28] J. Tropp, *J. Chem. Phys.* **1980,** *72,* 6035.

[29] G. Quinkert, N. Heim, J. Glenneberg, U. Döller, M. Eichhorn, U.-T. Billhardt, C. Schwarz, G. Zimmermann, J. W. Bats, G. Dürner, *Helv. Chim. Acta* **1988,** *71,* 1719.

[30] H. Kessler, D. F. Mierke, D. Donald, M. Furber, *Angew. Chem.* **1991,** *103,* 968.

[31] A. T. Hagler, in 'The Peptides'. Eds. S. Udenfried, J. Meienhofer, and V. Hruby, Academic Press, Orlando, Fl, Vol. 7, 1985, pp. 214–296.

[32] D. F. Mierke, H. Kessler, *J. Am. Chem. Soc.* **1991,** *113,* 9466–9470.

[33] W. F. van Gunsteren, R. Kaptein, E. R. P. Zuiderweg, 'Proceedings of the NATO/CECAM Workshop on Nucleic Acid Conformation and Dynamics'. Ed. W. K. Olsen, Orsay, 1983, pp. 79–92.

[34] T. M. G. Koning, R. Boelens, R. Kaptein, *J. Magn. Reson.* **1990,** *90,* 111.